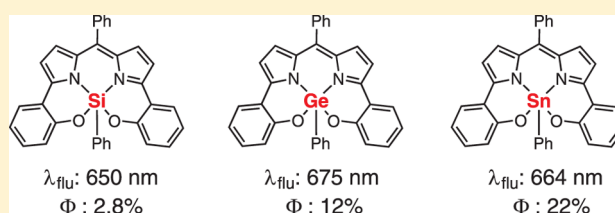


## Red/Near-Infrared Luminescence Tuning of Group-14 Element Complexes of Dipyrrens Based on a Central Atom

Masaki Yamamura,<sup>†</sup> Marcel Albrecht,<sup>‡</sup> Markus Albrecht,<sup>‡</sup> Yoshinobu Nishimura,<sup>†</sup> Tatsuo Arai,<sup>†</sup> and Tatsuya Nabeshima<sup>\*,†</sup><sup>†</sup>Graduate School of Pure and Applied Sciences & Tsukuba Research Center for Interdisciplinary Materials Science, University of Tsukuba, 1-1-1 Tennodai, Tsukuba, Ibaraki 305-8571, Japan<sup>‡</sup>Institut für Organische Chemie, RWTH Aachen University, Landoltweg 1, 52074 Aachen, Germany

## Supporting Information

**ABSTRACT:** A dipyrin complex has been one of the most utilized fluorescent dyes, and a variety of dipyrin complexes show intriguing functions based on the various coordination structures of the central element. We now report the synthesis, structure, and photophysical properties of germanium and stannane complexes of the N2O2-type tetradentate dipyrin, L•Ge and L•Sn, which are heavier analogues of the previously reported dipyrin silicon complex, L•Si. The central group-14 atoms of the monomeric complexes have geometries close to trigonal bipyramidal (TBP), in which the contribution of the square-pyramidal (SP) character becomes higher as the central atom is heavier. Interestingly, L•Sn formed a dimeric structure in the crystal. All complexes L•Si, L•Ge, and L•Sn showed a fluorescence in the red/NIR region. Fluorescence quantum yields of L•Ge and L•Sn are higher than that of L•Si. These results indicated that the central atom on the dipyrin complexes contributes not only to the geometry difference but also to tuning the fluorescence properties.

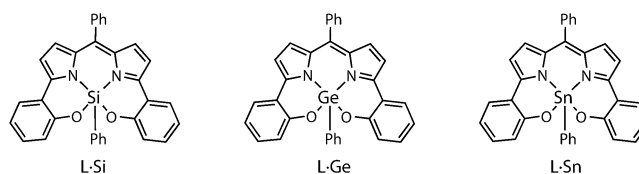


## INTRODUCTION

Development of fluorescent materials has been important for applications to fluorescent sensors, biolabels, and laser dyes. Among a huge number of fluorophores, a dipyrin–boron complex (BODIPY) has been one of the most utilized fluorescent dyes because of their sharp and intense absorption in the visible region, high fluorescent quantum yield, and high chemical and photochemical stability.<sup>1</sup> A variety of dipyrin complexes containing a central atom other than boron have been found to show intriguing functions based on the various coordination structures of the central element, for example, self-assembly,<sup>2</sup> anion sensing,<sup>3</sup> polymerization catalysis,<sup>4</sup> and detoxification of a biological oxidant.<sup>5</sup> We recently reported the first synthesis of dipyrin–silicon hypercoordinate complexes<sup>6</sup> and their strong luminescent properties utilizing the N2O2-type tetradentate dipyrins.<sup>7</sup> The hypercoordinate structure of the dipyrin–silicon complexes is stabilized by a chelate effect of the five-membered rings. The dipyrin–silicon complexes have a pentacoordinate silicon center (hypercoordinate structure) having one more substituent than the N2O2-type BODIPYs. As the hypercoordinate silicon compound features facile bond dissociation on the silicon center,<sup>8</sup> the dipyrin silicon complexes can be assembled and disassembled via bond formation and dissociation as follows: a dipyrin–silicon complex bearing a Si–OH group was dehydrated to form a dipyrin dimer bridged through a Si–O–Si bond. In addition, the dative Si–O–Si bond was reversibly dissociated and reformed to switch the red/NIR luminescence.

Recently, germanium and stannane complexes of the N2O2-type dipyrin, heavier analogues of the silicon complex, have been reported as polymerization catalysts.<sup>4</sup> However, their fluorescent properties have not been investigated. We now report the synthesis, structure, and photophysical properties of the germanium and stannane complexes (Chart 1). The notable finding in this study is the effect of the heavier atoms (Ge and Sn) on the red shift and enhancement of the fluorescence.

Chart 1. Dipyrin Complexes L•Si, L•Ge, and L•Sn



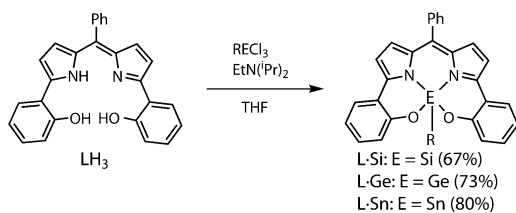
## RESULTS AND DISCUSSION

Silicon complex L•Si was synthesized by reaction of the N2O2-type ligand LH<sub>3</sub> with PhSiCl<sub>3</sub> in the presence of tertiary amine (Scheme 1).<sup>7</sup> The corresponding germanium and tin analogues, L•Ge and L•Sn, were similarly obtained using PhGeCl<sub>3</sub> and PhSnCl<sub>3</sub>, respectively.

Received: August 19, 2013

Published: January 14, 2014

Scheme 1



X-ray structural analysis of a single crystal of **L•Ge** revealed a distorted trigonal-bipyramidal (TBP) structure of the Ge center (Figure 1). One pyrrole and one phenoxy group of **L•Ge**

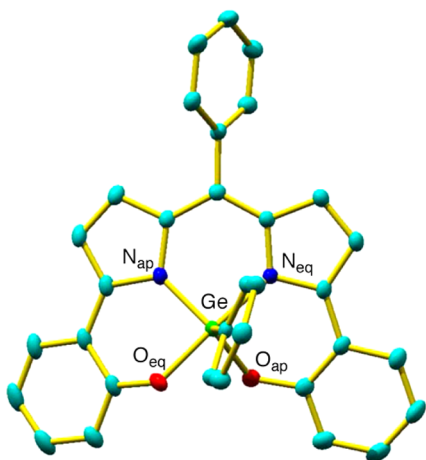


**Figure 1.** Perspective drawing of **L•Ge** (50% probability). Hydrogen atoms are omitted for clarity.

occupy the apical position of the TBP structure, and the other three groups lie at equatorial positions. A similar TBP geometry was observed in the silicon analogue **L•Si**. In contrast to **L•Si** and **L•Ge**, **L•Sn** has a dimeric structure in the crystal (Figure 2), which is formed by intermolecular Sn...O bonds (bond length 2.2537(18) Å). It is well known that many tin compounds having Sn–O bonds undergo aggregation through the Sn...O bonds (2.0–2.4 Å).<sup>9</sup> **L•Sn** has an octahedral Sn center having five valence bonds and one intermolecular Sn...O coordination

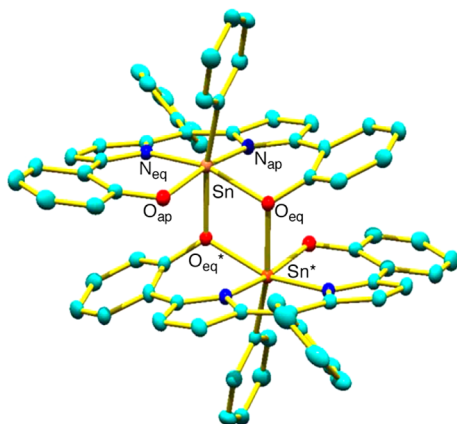


**Figure 2.** Perspective drawing of **L•Sn** (50% probability). Hydrogen atoms and solvent molecule are omitted for clarity. Oxygen atom involved in the intramolecular coordination is tentatively defined as the  $\text{O}_{\text{eq}}$  of **L•Sn**, here.

bond. The reported N2O2-dipyrin germanium and stannane complexes similarly adopted TBP and octahedral structures, respectively.<sup>4</sup> A direct structural comparison of **L•Ge** and **L•Sn** is difficult because their coordination numbers are different. Monomeric structures of **L•Si**, **L•Ge**, and **L•Sn** were optimized by DFT calculations.<sup>10</sup> Structural parameters obtained by the X-ray analysis and DFT calculations are summarized in Table 1.

The  $\text{N}_{\text{ap}}-\text{Ge}-\text{O}_{\text{ap}}$  angle ( $167.65(5)^\circ$  (X-ray) and  $166.08^\circ$  (calcd)) of **L•Ge** is distorted from the idealized value ( $180^\circ$ ) of the TBP structure, whereas the silicon analogue **L•Si** has  $\text{N}_{\text{ap}}-\text{Si}-\text{O}_{\text{ap}}$  angles ( $177.80(9)^\circ$  (X-ray) and  $172.73^\circ$  (calcd)) closer to  $180^\circ$ . The  $\text{N}_{\text{ap}}-\text{Sn}-\text{O}_{\text{ap}}$  angle ( $163.08^\circ$ ) of the calculated **L•Sn** is narrower than that of **L•Ge**. Contrary to the  $\text{N}_{\text{ap}}-\text{E}-\text{O}_{\text{ap}}$  angles, the  $\text{N}_{\text{eq}}-\text{E}-\text{O}_{\text{eq}}$  angles widen in the order **L•Si** ( $123.28^\circ$ ) < **L•Ge** ( $125.72^\circ$ ) < **L•Sn** ( $127.87^\circ$ ) in the calculated structures. The distortions of these two angles are indicative of the contribution of the square-pyramidal (SP) character. In the three compounds, the  $\text{N}_{\text{eq}}-\text{E}-\text{O}_{\text{eq}}$  of **L•Si** is the closest angle to that of TBP ( $120^\circ$ ). In order to evaluate the SP contributions, the  $\tau$  values were calculated:  $\tau = 1$  for an idealized TBP and  $\tau = 0$  for an SP.<sup>11</sup>  $\tau$  values based on the calculated structures were 0.82, 0.67, and 0.59 for **L•Si**, **L•Ge**, and **L•Sn**, respectively, which indicated that the order of the SP character is in the order **L•Si** < **L•Ge** < **L•Sn**.

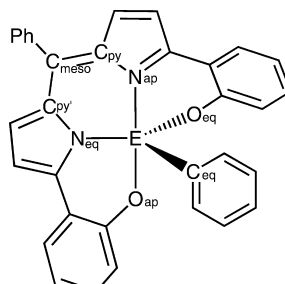
One more striking structural difference is the bite angle on the methine carbon bridging the two pyrrole rings ( $\text{C}_{\text{py}}-\text{C}_{\text{meso}}-\text{C}_{\text{py}'}$ ). The bite angles become larger in the order **L•Si** < **L•Ge** < **L•Sn** in both the experimental (**L•Si**  $120.8(2)^\circ$ , **L•Ge**  $123.2(2)^\circ$ , and **L•Sn**  $126.5(2)^\circ$ ) and the calculated (**L•Si**  $121.2^\circ$ , **L•Ge**  $122.7^\circ$ , and **L•Sn**  $125.0^\circ$ ) structures.

Although the two pyrroles of **L•Si**, **L•Ge**, and **L•Sn** are nonequivalent in the crystal and calculated structures, the pyrrole units are equivalent in the  $^1\text{H}$  and  $^{13}\text{C}$  NMR spectra.<sup>6</sup> This fact suggests that the pyrroles at the apical and equatorial positions are exchangeable according to the Berry pseudorotation mechanism.<sup>12</sup>

Absorption spectra of **L•Si**, **L•Ge**, and **L•Sn** were measured in chloroform. Silicon complex **L•Si** showed an intense absorption at 612 nm along with a shoulder ascribed to a vibrational band (Figure 3, Table 2).<sup>6</sup> The absorption spectral shape of **L•Sn** was very similar to **L•Si**, but absorption of **L•Sn** was observed in the red-shifted region (maximum 637 nm). Absorption of **L•Ge** is broader, and the maximum value is intermediate (620 nm) between those of **L•Si** and **L•Sn**.

TD DFT calculations were performed to clarify the excitations of the dipyrin complexes.<sup>15</sup> The excitation energies to the  $\text{S}_1$  states for **L•Si**, **L•Ge** and **L•Sn** were determined to be 2.429 eV ( $f = 0.43$ ), 2.402 eV ( $f = 0.45$ ), and 2.431 eV ( $f = 0.52$ ), respectively (Table 3). All  $\text{S}_1$  excitations of the three compounds are assigned to the HOMO–LUMO transitions with more than 97% contributions. The frontier Kohn–Sham orbitals of the three complexes are very similar to each other, and none of them includes the atomic orbitals of the central atoms (Figure 4). The frontier orbital energies of **L•Si** are the lowest among the three. This prediction was reproduced by cyclic voltammetry (CV) measurements (Table 4, Figures S1–S3, Supporting Information). CV of all complexes, **L•Si**, **L•Ge**, and **L•Sn**, exhibited one reversible one-electron reduction wave with  $\Delta E_p$  values of  $\sim 70$  mV and two quasi-reversible one-electron oxidation waves with  $\Delta E_p$  values in the range of 80–97 mV at 100 mV/s. Electrochemical parameters are summarized in Table 4. Both the oxidation and the reduction potential of **L•**

Table 1. Coordination Parameters of Pentacoordinate Dipyrin Complexes L·Si, L·Ge, and L·Sn



	L·Si		L·Ge		L·Sn	
	X-ray <sup>6</sup>	calcd	X-ray	calcd	X-ray <sup>a</sup> (octahedral)	calcd (TBP)
bond lengths (Å)						
N <sub>ap</sub> –E	1.904(2)	1.922	1.976(2)	1.996	2.125(2)	2.130
N <sub>eq</sub> –E	1.807(2)	1.847	1.919(2)	1.924	2.117(2)	2.100
O <sub>ap</sub> –E	1.732(2)	1.742	1.859(1)	1.880	2.0234(18)	1.975
O <sub>eq</sub> –E	1.688(2)	1.708	1.825(1)	1.842	2.1077(17)	1.963
C <sub>eq</sub> –E	1.828(3)	1.894	1.939(2)	1.935	2.147(3)	2.101
O <sub>ap</sub> ...E (intermolecular)					2.2537(18)	
bond angles (deg)						
N <sub>ap</sub> –E–O <sub>ap</sub>	177.80(9)	172.73	167.65(5)	166.08	166.97(8)	163.08
N <sub>ap</sub> –E–N <sub>eq</sub>	88.22(9)	87.00	88.12(5)	87.43	86.79(8)	84.00
N <sub>ap</sub> –E–O <sub>eq</sub>	88.50(9)	88.00	86.71(5)	86.80	84.21(8)	84.50
N <sub>ap</sub> –E–C <sub>eq</sub>	90.56(10)	93.61	97.14(5)	98.18	97.40(9)	97.55
O <sub>ap</sub> –E–N <sub>eq</sub>	91.61(9)	90.71	90.29(5)	90.21	89.40(8)	87.94
O <sub>ap</sub> –E–O <sub>eq</sub>	89.72(9)	87.50	84.93(5)	83.46	94.17(7)	88.78
O <sub>ap</sub> –E–C <sub>eq</sub>	91.38(10)	93.63	94.65(5)	95.24	95.62(9)	99.31
N <sub>eq</sub> –E–O <sub>eq</sub>	121.45(10)	123.28	129.93(5)	125.72	155.00(8)	127.87
N <sub>eq</sub> –E–C <sub>eq</sub>	123.00(12)	113.38	114.71(5)	115.23	106.66(9)	113.60
O <sub>eq</sub> –E–C <sub>eq</sub>	115.45(12)	123.32	115.35(5)	119.02	97.62(8)	118.26
C <sub>py</sub> –C <sub>meso</sub> –C <sub>py</sub>	120.8(2)	121.2	123.2(2)	122.7	126.5(2)	125.0

<sup>a</sup>Apical and equatorial positions of the octahedral L·Sn are defined as shown in Figure 2.

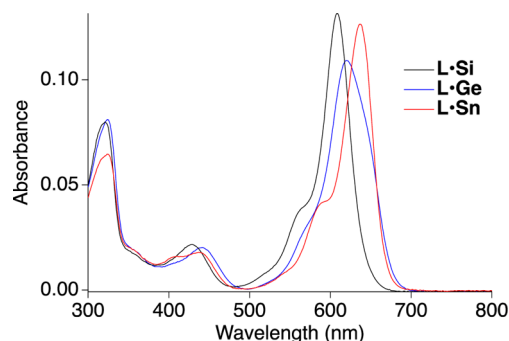


Figure 3. UV–vis absorption spectra of L·Si<sup>6</sup> (black), L·Ge (blue), and L·Sn (red) in CHCl<sub>3</sub> (3 μM).

Si are the highest among the three, as expected from the calculations.

Table 3. Singlet Electronic Excitation of L·Si, L·Ge, and L·Sn Based on TD DFT Using the M06-2X Functional

	transition states	calcd (eV)	exp. (eV)
L·Si	S <sub>1</sub> (97% HOMO–LUMO)	2.429 ( <i>f</i> = 0.43)	2.01
	S <sub>2</sub> (96% HOMO-1–LUMO)	3.406 ( <i>f</i> = 0.23)	2.87
	S <sub>3</sub> (84% HOMO-2–LUMO)	3.850 ( <i>f</i> = 0.03)	3.85
L·Ge	S <sub>1</sub> (98% HOMO–LUMO)	2.402 ( <i>f</i> = 0.45)	1.99
	S <sub>2</sub> (96% HOMO-1–LUMO)	3.322 ( <i>f</i> = 0.21)	2.83
	S <sub>3</sub> (91% HOMO-2–LUMO)	3.750 ( <i>f</i> = 0.06)	3.84
L·Sn	S <sub>1</sub> (98% HOMO–LUMO)	2.431 ( <i>f</i> = 0.52)	1.94
	S <sub>2</sub> (96% HOMO-1–LUMO)	3.400 ( <i>f</i> = 0.21)	2.85
	S <sub>3</sub> (92% HOMO-2–LUMO)	3.750 ( <i>f</i> = 0.07)	3.84

Fluorescence spectra of L·Si, L·Ge, and L·Sn were measured in chloroform with the excitation at 550 nm. All fluorescence spectra of these complexes were mirror images of the

Table 2. Spectroscopic and Photophysical Data of L·Si, L·Ge, and L·Sn

	absorption		fluorescence				
	λ <sub>abs</sub> /nm	ε/cm <sup>-1</sup> ·M <sup>-1</sup>	λ <sub>flu</sub> /nm	τ <sub>0</sub> /ns	Φ <sup>a</sup>	k <sub>r</sub> × 10 <sup>-7</sup> /s <sup>-1</sup>	k <sub>nr</sub> × 10 <sup>-7</sup> /s <sup>-1</sup>
L·Si	612 <sup>b</sup>	4.4 × 10 <sup>4</sup>	650 <sup>b</sup>	0.18	0.028 <sup>b</sup> (0.028)	16	550
L·Ge	620	3.5 × 10 <sup>4</sup>	675	1.9	0.12 (0.13)	6.9	45
L·Sn	637	4.2 × 10 <sup>4</sup>	664	3.2	0.22	6.9	25

<sup>a</sup>Quantum yields were determined by the absolute method using an integrating sphere instrument.<sup>13</sup> The parentheses values of L·Si and L·Ge are quantum yields determined by the relative method using L·Sn as a standard.<sup>14</sup> <sup>b</sup>Reference 14.

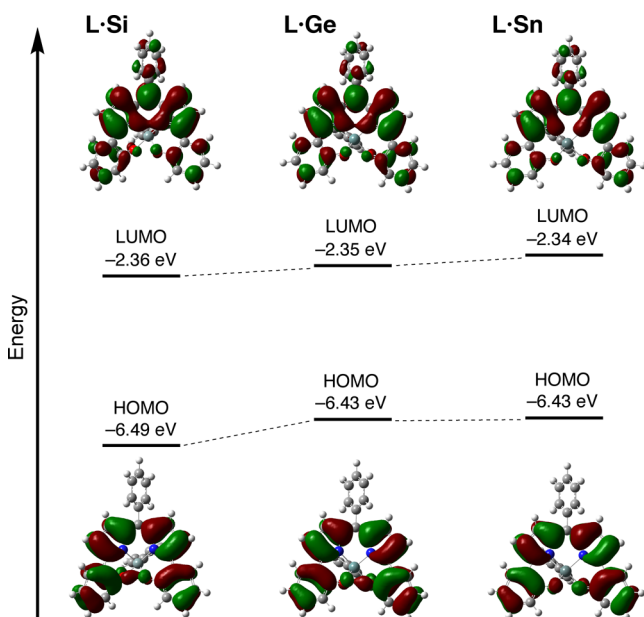


Figure 4. Frontier Kohn–Sham orbitals of L·Si, L·Ge, and L·Sn.

Table 4. Electrochemical Data of L·Si, L·Ge, and L·Sn

	electrochemical data/V ( $\Delta E_p/mV$ ) <sup>a</sup>		
	$E_{1/2}^{red}$	$E_{1/2}^{ox1}$	$E_{1/2}^{ox2}$
L·Si	-1.131 (74)	0.826 (80)	1.082 (90)
L·Ge	-1.436 (72)	0.397 (90)	0.848 (89)
L·Sn	-1.422 (70)	0.512 (82)	0.995 (97)

<sup>a</sup>Potentials versus Fc/Fc<sup>+</sup> = 0.20 V in 0.1 M Bu<sub>4</sub>NClO<sub>4</sub>/CH<sub>2</sub>Cl<sub>2</sub>. Scan rate: 100 mV/s. Glassy carbon working, platinum wire counter, and Ag/Ag<sup>+</sup> reference electrodes.  $E_{1/2} = (E_{pa} + E_{pc})/2$ ,  $\Delta E_p = E_{pa} - E_{pc}$ .

corresponding absorption spectra (Figure 5). The fluorescence of L·Sn is slightly red shifted compared to L·Si. L·Ge has the

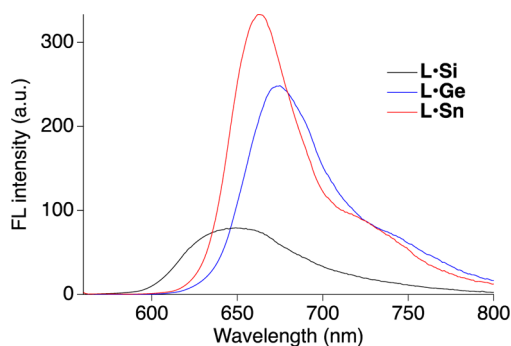


Figure 5. FL spectra of L·Si (black), L·Ge (blue), and L·Sn (red) in CHCl<sub>3</sub> (3 μM,  $\lambda_{ex}$  = 550 nm).

longest fluorescence wavelength (675 nm) of the three complexes (Table 2). Noteworthy is that the fluorescence quantum yields are also significantly dependent on the central atom. The quantum yield of L·Si is very low (2.8%) because the internal rotation of the *meso*-Ph group should cause an efficient nonradiative decay.<sup>16</sup> This prediction is suggested by the LUMO orbitals that contain the orbitals on the *meso*-Ph group.<sup>17</sup> The delocalization of the LUMO orbital to the *meso*-Ph group is responsible for the decrease in the transition energy upon the Ph ring rotation. Thus, the excitation energy is

converted to the nonradiative rotation energy of the *meso*-Ph group.

Although the contributions of the *meso*-Ph group to the LUMOs of the three compounds are almost the same, L·Ge and L·Sn have higher quantum yields, 12% and 22%, respectively, than L·Si. This is probably because the wider C<sub>py</sub>–C<sub>meso</sub>–C<sub>py</sub> bite angles in L·Ge and L·Sn force the two pyrroles closer to the *meso*-Ph group, which inhibit internal rotation of *meso*-Ph. Rate constants for S<sub>1</sub> to S<sub>0</sub> decay via radiative ( $k_r$ ) and nonradiative ( $k_{nr}$ ) processes are determined by the fluorescence quantum yields and lifetimes ( $\tau_0$ , Table 2). Radiative rate constants ( $k_r$ ) are in a range typical of BODIPY analogues.<sup>16</sup> There is a definite correlation between the nonradiative rate constants ( $k_{nr}$ ) and the bite angles of L·Si, L·Ge, and L·Sn, supporting the assumption that the large bite angle inhibits rotation of the *meso*-Ph group.

In summary, the germanium and stannane complexes of the N2O2-type dipyrin were synthesized. Structures of the dipyrin group-14 complexes were studied by X-ray analysis and DFT calculations. The central group-14 atoms of the monomeric complexes have geometries close to TBP, in which the contribution of the SP character becomes higher as the central atom is heavier. Interestingly, L·Sn formed a dimeric structure in the crystal. All complexes showed a fluorescence in the red/NIR region in CHCl<sub>3</sub>. Fluorescence wavelengths of L·Ge and L·Sn are red shifted compared to that of L·Si. Furthermore, fluorescence quantum yields increase according to the order of the periodic table. These results indicated that the central atom on the dipyrin complexes contributes not only to the geometry difference but also to tuning of the fluorescence properties. These findings should be important in the design of advanced red/NIR fluorescent materials.

## EXPERIMENTAL SECTION

**General.** All chemicals were reagent grade and used without further purification. All reactions were performed under a nitrogen atmosphere. Melting points were determined using a Yanaco and are uncorrected. <sup>1</sup>H NMR spectra were recorded on a Varian Inova 400 at 400 MHz. <sup>13</sup>C NMR spectra were recorded by a Varian Inova 400 at 100 MHz. In these NMR measurements, tetramethylsilane was used as the internal standard (0 ppm). IR spectra were recorded by a PE-1760FT spectrometer. High-resolution mass spectra (ESI-TOF, positive mode) were recorded by a Thermo Finnigan LCQ Deca XP Plus and ThermoFischer Scientific LTQ Orbitrap XL.

**Synthesis of L·Ge.** To a solution of 1,9-bis(2-hydroxyphenyl)-5-(phenyl)dipyrin (LH<sub>3</sub>)<sup>18</sup> (40 mg, 0.1 mmol) in 20 mL of dry THF were added *N,N*-diisopropylethylamine (0.34 mL, 2.0 mmol) and phenylgermanium trichloride (77 mg, 0.3 mmol). The mixture was stirred at room temperature for 40 h; then 4 mL of methanol was added. After evaporation of the solvent, the crude product was dissolved in dichloromethane (20 mL) and washed with a saturated aqueous Na<sub>2</sub>CO<sub>3</sub> solution. After drying over MgSO<sub>4</sub> and evaporation of the solvent, crude product was purified by column chromatography (neutral alumina, CH<sub>2</sub>Cl<sub>2</sub>). P product was isolated as a green metallic solid of L·Ge (34 mg, 73%).

Mp 259–260 °C. <sup>1</sup>H NMR (400 MHz, CDCl<sub>3</sub>):  $\delta$  6.86 (td,  $J$  = 1.3, 7.5 Hz, 2H), 6.88 (d,  $J$  = 4.5 Hz, 2H), 7.00 (d,  $J$  = 4.5 Hz, 2H), 7.14–7.25 (m, 7H), 7.29 (td,  $J$  = 1.6, 7.6 Hz, 2H), 7.44–7.63 (m, 5H), 7.62 (dd,  $J$  = 1.6, 4.0 Hz, 2H). <sup>13</sup>C NMR (100 MHz, CDCl<sub>3</sub>):  $\delta$  115.5, 117.0, 119.2, 121.5, 127.0, 127.9, 128.3, 129.3, 130.3, 130.6, 131.8, 132.3, 133.6, 135.9, 136.2, 139.3, 139.6, 158.6, 161.8. IR (KBr):  $\nu$  (cm<sup>-1</sup>) 3053, 1601, 1546, 1492, 1428, 1333, 1242, 1198, 1124, 1059, 1026, 933, 849, 788, 749, 690. ESI-TOF MS observed  $m/z$ : 575.07861 [M + Na]<sup>+</sup>, calcd for C<sub>33</sub>H<sub>22</sub>O<sub>2</sub>N<sub>2</sub>GeNa 575.07853. Anal. Calcd for C<sub>33</sub>H<sub>22</sub>N<sub>2</sub>O<sub>2</sub>Ge: C, 71.91; H, 4.02; N, 5.08. Found: C, 71.48; H, 3.78; N, 4.94.

**Synthesis of L•Sn.** To a solution of 1,9-bis(2-hydroxyphenyl)-5-(phenyl)dipyrrin (LH<sub>3</sub>) (40 mg, 0.1 mmol) in 20 mL of dry THF were added *N,N*-diisopropylethylamine (0.34 mL, 2.0 mmol) and phenyltin trichloride (91 mg, 0.3 mmol). The mixture was stirred at room temperature for 20 h; then 4 mL of methanol was added. After evaporation of the solvent, crude product was purified by column chromatography (neutral alumina, CH<sub>2</sub>Cl<sub>2</sub>:MeOH, 2:1). Product was isolated as a green metallic solid of L•Sn (48 mg, 80%).

Mp > 300 °C. <sup>1</sup>H NMR (400 MHz, CDCl<sub>3</sub>): δ 6.71 (d, *J* = 4.5 Hz, 2H), 6.76 (td, *J* = 1.1, 7.5 Hz, 2H), 6.91 (d, *J* = 4.5 Hz, 2H), 7.06 (d, *J* = 8.3 Hz, 2H), 7.17 (td, *J* = 1.6, 7.7 Hz, 2H), 7.23–7.30 (m, 5H), 7.43 (m, 2H), 7.49–7.52 (m, 5H). <sup>13</sup>C NMR (100 Hz, CDCl<sub>3</sub>): δ 116.7, 118.4, 119.1, 123.1, 127.6, 127.7, 128.2, 128.9, 128.9, 130.6, 131.8, 133.7, 135.2, 137.1, 137.1, 140.1, 140.7, 160.4, 162.1. IR(KBr): ν (cm<sup>-1</sup>) 3060, 2853, 2115, 1599, 1534, 1482, 1429, 1327, 1296, 1257, 1195, 1123, 1083, 1055, 1023, 846, 790, 752, 718. ESI-TOF MS obsd *m/z* 637.03259 [M + K]<sup>+</sup>, calcd for C<sub>33</sub>H<sub>22</sub>O<sub>2</sub>N<sub>2</sub>KSn 637.03348. Anal. Calcd for C<sub>33</sub>H<sub>22</sub>N<sub>2</sub>O<sub>2</sub>Sn•0.5CH<sub>2</sub>Cl<sub>2</sub>: C, 62.90; H, 3.62; N, 4.38. Found: C, 63.07; H, 3.32; N, 4.23.

**X-ray Crystallography.** X-ray diffraction measurements of L•Ge and L•Sn were performed using a Bruker APEXII ULTRA. X-ray diffraction intensities were collected on a CCD diffractometer at 120 K using Mo Kα (graphite monochromated, λ = 0.71073 Å) radiation. Data were integrated with SAINT (Bruker, 2004), and an empirical absorption correction (SADABS)<sup>19</sup> was applied. The structure was solved by the direct or Peterson method of SHELXS-97 and refined using the SHELXL-97 program.<sup>20</sup> All of the positional parameters and thermal parameters of non-hydrogen atoms were anisotropically refined on F<sup>2</sup> by the full-matrix least-squares method. Hydrogen atoms were placed at the calculated positions and refined riding on their corresponding carbon atoms. Crystallographic data for L•Ge and L•Sn were deposited with the Cambridge Crystallographic Data Center as supplementary publications CCDC-955085 and 955086, respectively. Copies of the data can be obtained free of charge on application to CCDC, 12 Union Road, Cambridge CB2 1EZ, U.K. (fax (+44) 1223-336-033; email deposit@ccdc.cam.ac.uk).

**Electrochemical Studies.** Cyclic voltammograms were recorded by a BAS ALS/CHI model 750A. A Ag/AgNO<sub>3</sub> reference electrode was used. The working electrode was a 1-mm-diameter glassy carbon with a platinum wire acting as the counter electrode. CV measurement was taken at a scan rate of 100 mV/s. After measurements in 0.1 M Bu<sub>4</sub>NClO<sub>4</sub>/CH<sub>2</sub>Cl<sub>2</sub> without any internal reference, ferrocene was added to the same sample and the electrochemical potential was adjusted to ferrocenium/ferrocene as the internal reference (Fc/Fc<sup>+</sup> = 0.0 V).

**Photophysical Studies.** UV–vis absorption spectra were recorded by a JASCO V-660 spectrophotometer. Fluorescence spectra and absolute quantum yields were recorded by a JASCO FP-8600 spectrometer and a Hamamatsu Photonics absolute PL quantum yield measurement system C9920-02, respectively.<sup>13</sup> Fluorescence decay measurements were performed using a time-correlated single-photon counting method.<sup>21</sup> Laser excitation at 410 nm was achieved using a diode laser (PicoQuant, LDH-P-C-405) with a power control unit (PicoQuant, PDL 800-B) in a repetition rate of 2.5 MHz. Temporal profiles of fluorescence decay were detected using a microchannel plate photomultiplier (Hamamatsu, R3809U) equipped with a TCSPC computer board module (Becker and Hickl, SPC630). Full-width at half-maximum (fwhm) of the instrument response function was 51 ps. Values of χ<sup>2</sup> and Durbin–Watson parameters were used to determine the quality of the fit obtained by nonlinear regression.<sup>22</sup>

**Computational Methods.** DFT calculations were performed using the Gaussian09 packages<sup>23</sup> with the M06-2X functional.<sup>10</sup> Basis sets 6-31G(d,p) for C, H, N, O, Si, and Ge and LANL2DZ for Sn were used for geometry optimizations and vibrational analysis, and 6-311++G(d,p) for C, H, N, O, Si, and Ge and LANL2DZ for Sn were used for time-dependent calculations. The effective core potential<sup>24</sup> was included in LANL2DZ basis sets.

## ■ ASSOCIATED CONTENT

### ■ Supporting Information

X-ray crystallographic data, details of electrochemical and photochemical experiments, DFT calculations, and CIF files. This material is available free of charge via the Internet at <http://pubs.acs.org>.

## ■ AUTHOR INFORMATION

### Corresponding Author

\*E-mail: nabesima@chem.tsukuba.ac.jp.

### Notes

The authors declare no competing financial interest.

## ■ ACKNOWLEDGMENTS

This research was financially supported by Grants-in-Aid for Scientific Research from the Ministry of Education, Culture, Sports, Science, and Technology of Japan and by the Tokyo Biochemical Research Foundation.

## ■ REFERENCES

- (1) (a) Treibs, A.; Kreuzer, F.-H. *Justus Liebig's Ann. Chem.* **1968**, 718, 208. (b) Loudet, A.; Burgess, K. *Chem. Rev.* **2007**, 107, 4891. (c) Ulrich, G.; Ziesse, R.; Harriman, A. *Angew. Chem., Int. Ed.* **2008**, 47, 1184.
- (2) (a) Zhang, Y.; Thompson, A.; Rettig, S. J.; Dolphin, D. *J. Am. Chem. Soc.* **1998**, 120, 13537. (b) Yu, L.; Muthukumar, K.; Sazanovich, I. V.; Kirmaier, K.; Hindin, E.; Diers, J. R.; Boyle, P. D.; Bocian, D. F.; Holten, D.; Lindsey, J. S. *Inorg. Chem.* **2003**, 42, 6629. (c) Wood, T. E.; Dalgleish, N. D.; Power, E. D.; Thompson, A.; Chen, X.; Okamoto, Y. *J. Am. Chem. Soc.* **2005**, 127, 5740. (d) Béziau, A.; Baudron, S. A.; Guenet, A.; Hosseini, M. W. *Chem.—Eur. J.* **2013**, 19, 3215.
- (3) Kobayashi, J.; Kushida, T.; Kawashima, T. *J. Am. Chem. Soc.* **2009**, 131, 10836.
- (4) Nakano, K.; Kobayashi, K.; Nozaki, K. *J. Am. Chem. Soc.* **2011**, 133, 10720.
- (5) Rausaria, S.; Kamadulski, A.; Rath, N. P.; Bryant, L.; Chen, Z.; Salvemini, D.; Neumann, A. L. *J. Am. Chem. Soc.* **2011**, 133, 4200.
- (6) Sakamoto, N.; Ikeda, C.; Yamamura, M.; Nabeshima, T. *J. Am. Chem. Soc.* **2011**, 133, 4726.
- (7) (a) Bloom, S. M.; Garcia, P. P. US Pat. 3,691,161, 1972. (b) Kim, H.; Burghart, A.; Welch, M. B.; Reibenspies, J.; Burgess, K. *Chem. Commun.* **1999**, 1889.
- (8) (a) Corriu, R. J. P.; Young, J. C. In *The Chemistry of Organic Silicon Compounds*; Patai, S., Rappoport, Z., Eds.; John Wiley & Sons: Britain, 1989, 1241. (b) Hosomi, A. *Acc. Chem. Res.* **1988**, 21, 200. (c) Chuit, C.; Corriu, R. J. P.; Reye, C.; Young, J. C. *Chem. Rev.* **1993**, 93, 1371. (d) Holmes, R. R. *Chem. Rev.* **1990**, 90, 17.
- (9) (a) Smith, P. J.; White, R. F. M.; Smith, L. J. *Organomet. Chem.* **1972**, 40, 341. (b) Choi, J.-C.; Sakakura, T.; Sako, T. *J. Am. Chem. Soc.* **1999**, 121, 3793. (c) Whittleton, S. R.; Rolle, A. J.; Boyd, R. J.; Grindley, T. B. *Organometallics* **2010**, 29, 6384.
- (10) In the preliminary calculations of L•Si and L•Ge, the M06-2X functional affords the best results among the various functionals (B3LYP, PBE1PBE, B3PW91, and X3LYP), which are closest to the experimental values. Thus, geometry optimization of L•Sn was performed by utilizing the M06-2X functional with 6-31G(d,p) basis set for C, H, N, and O and LANL2DZ for Sn. M06-2X functional: Zhao, Y.; Truhlar, D. G. *Theor. Chem. Acc.* **2008**, 120, 215.
- (11) Addison, A. W.; Rao, T. N.; Reedijk, J.; van Rijn, J.; Verschoor, G. C. *J. Chem. Soc., Dalton. Trans.* **1984**, 1349.
- (12) Berry, R. S. *J. Chem. Phys.* **1960**, 32, 933.
- (13) (a) Suzuki, K.; Kobayashi, A.; Kaneko, S.; Takehira, K.; Yoshihara, T.; Ishida, H.; Shiina, Y.; Oishi, S.; Tobita, S. *Phys. Chem. Chem. Phys.* **2009**, 11, 9850. (b) Ishida, H.; Tobita, S.; Hasegawa, Y.; Katoh, R.; Nozaki, K. *Coord. Chem. Rev.* **2010**, 254, 2449.

(14) The  $\lambda_{\max}$  value of L•Si (650 nm) is a little different from the previous reported one (660 nm). See ref 6. In this study, the spectral difference was observed after repeated recrystallization of L•Si. Fluorescence decay of the recrystallized sample showed a single component (Figure S6, Supporting Information), indicating the high purity of L•Si in spectroscopic grade. The high purity of L•Ge and L•Sn was also supported by the fluorescence decay (Figures S7 and S8, Supporting Information).

(15) Calculation methods for the excitation states of the dipyrin complex derivatives have been thoroughly tested. We selected M06-2X, which is the most adequate functional predicting a reliable excitation state consistent with experimental results. Generally, the theoretical transition energies in this calculation are much higher than the experimental ones. However, the systematically constant deviation enables a comparison of the different derivatives. Although the energy differences among the three complexes are so small that the calculated  $S_1$  excitation energy is not comparable to the experimental value, deviations in our compounds are within acceptable limits. See: Chibani, S.; Le Guennic, B.; Charaf-Eddin, A.; Laurenta, A. D.; Jacquemin, D. *Chem. Sci.* **2013**, *4*, 1950.

(16) (a) Li, F.; Yang, S. I.; Ciringh, Y.; Seth, J.; Martin, C. H., III; Singh, D. L.; Kim, D.; Birge, R. R.; Bocian, D. F.; Holten, D.; Lindsey, J. S. *J. Am. Chem. Soc.* **1998**, *120*, 10001. (b) Sazanovich, I. V.; Kirmaier, C.; Hindin, E.; Yu, L.; Bocian, D. F.; Lindsey, J. S.; Holten, D. *J. Am. Chem. Soc.* **2004**, *126*, 2664. (c) Kee, H. L.; Kirmaier, C.; Yu, L.; Thamyongkit, P.; Youngblood, W. J.; Calder, M. E.; Ramos, L.; Noll, B. C.; Bocian, D. F.; Scheidt, W. R.; Birge, R. R.; Lindsey, J. S.; Holten, D. *J. Phys. Chem. B* **2005**, *109*, 20433.

(17) At 77 K in THF/CH<sub>2</sub>Cl<sub>2</sub> (2:3 v/v) glass matrix under aerobic conditions all complexes showed emission spectra similar to those at room temperature (Figure S4, Supporting Information).

(18) Ikeda, C.; Ueda, S.; Nabeshima, T. *Chem. Commun.* **2009**, 2544.

(19) Sheldrick, G. M. *SADABS, Program for empirical absorption correction*; Universität Göttingen: Göttingen, Germany, 1996.

(20) Sheldrick, G. M. *SHELX97, Program for crystal structure determination*; Universität Göttingen: Göttingen, Germany, 1997.

(21) Nishimura, Y.; Kamada, M.; Ikegami, M.; Nagahata, R.; Arai, T. *J. Photochem. Photobiol. A* **2006**, *178*, 150.

(22) Boens, N.; Tamai, N.; Yamazaki, I.; Yamazaki, T. *Photochem. Photobiol.* **1990**, *52*, 911.

(23) Frisch, M. J.; Trucks, G. W.; Schlegel, H. B.; Scuseria, G. E.; Robb, M. A.; Cheeseman, J. R.; Scalmani, G.; Barone, V.; Mennucci, B.; Petersson, G. A.; Nakatsuji, H.; Caricato, M.; Li, X.; Hratchian, H. P.; Izmaylov, A. F.; Bloino, J.; Zheng, G.; Sonnenberg, J. L.; Hada, M.; Ehara, M.; Toyota, K.; Fukuda, R.; Hasegawa, J.; Ishida, M.; Nakajima, T.; Honda, Y.; Kitao, O.; Nakai, H.; Vreven, T.; Montgomery, Jr., J. A.; Peralta, J. E.; Ogliaro, F.; Bearpark, M.; Heyd, J. J.; Brothers, E.; Kudin, K. N.; Staroverov, V. N.; Keith, T.; Kobayashi, R.; Normand, J.; Raghavachari, K.; Rendell, A.; Burant, J. C.; Iyengar, S. S.; Tomasi, J.; Cossi, M.; Rega, N.; Millam, J. M.; Klene, M.; Knox, J. E.; Cross, J. B.; Bakken, V.; Adamo, C.; Jaramillo, J.; Gomperts, R.; Stratmann, R. E.; Yazyev, O.; Austin, A. J.; Cammi, R.; Pomelli, C.; Ochterski, J. W.; Martin, R. L.; Morokuma, K.; Zakrzewski, V. G.; Voth, G. A.; Salvador, P.; Dannenberg, J. J.; Dapprich, S.; Daniels, A. D.; Farkas, O.; Foresman, J. B.; Ortiz, J. V.; Cioslowski, J.; Fox, D. J. *GAUSSIAN 09, Revision A.02*; Gaussian, Inc.: Wallingford CT, 2009.

(24) (a) Hay, P. J.; Wadt, W. R. *J. Chem. Phys.* **1985**, *82*, 270.

(b) Wadt, W. R.; Hay, P. J. *J. Chem. Phys.* **1985**, *82*, 284. (c) Hay, P. J.; Wadt, W. R. *J. Chem. Phys.* **1985**, *82*, 299.